Version of Record: https://www.sciencedirect.com/science/article/pii/S1364682617300962
Manuscript_9ee6fb56a0a1b432375b4515743d3e1b

Statistical Analysis of Midlatitude Spread F using Multi-Station Digisonde Observations

P. Bhaneja, G.D. Earle[1], T.W. Bullett[2]

[1]Virginia Polytechnic Institute and State University, Blacksburg, VA, USA

[2]Cooperative Institute for Research in Environmental Sciences, NOAA/NGDC, Boulder, Colorado, USA

Abstract

A comprehensive statistical study of midlatitude spread F (MSF) is presented for five midlatitude stations in the North American sector. These stations include Ramey AFB, Puerto Rico (18.5°N, 67.1°W, -14° declination angle), Wallops Island, Virginia (37.95°N, 75.5°W, -11° declination angle), Dyess, Texas (32.4°N, 99.8°W, 6.9° declination angle), Boulder, Colorado (40°N, 105.3°W, 10° declination angle), and Vandenberg AFB, California (34.8°N,120.5°W, 13° declination angle). Pattern recognition algorithms are used to determine the presence of both range and frequency spread F. Data from 1996-2011 are analyzed, covering all of Solar Cycle 23 and the beginning of Solar Cycle 24. Variations with respect to season and solar activity are presented, including the effects of the extended minimum between cycles 23 and 24.

1. Introduction

Midlatitude F region in the ionosphere is known to exhibit anomalies and irregularities as observed in the perturbations in the electron density values. Gravity waves and traveling ionospheric disturbances (TIDs) are considered to be a seeding mechanism which create density perturbations in the ionosphere leading to spread F at midlatitude regions [*Kelley & Fukao, 1991; Oliver et al., 1994; Kazimirovsky et al.,* 2002; *Lastovicka*, 2006; *Rishbeth*, 2006]. *Hines* [1960] established a connection between traveling ionospheric disturbances (TIDs) and gravity waves. *Bowman* [1990] conducted a study using digisonde data from Birbie Island and Moggill (both are near Brisbane, Australia) and found a strong correlation between daytime TIDs and nighttime spread F. Atmospheric buoyancy waves, commonly referred to as gravity waves are generated from a variety of sources, including thunderstorms [*Wickwar & Carlson*, 1999; *Boska & Pauli*, 2001; *Walterscheid et al.,* 2001; *Kazimirovsky*, 2002; *Pulinets & Liu*, 2004; *Lasovicka*, 2006; *Rishbeth*, 2006; *Lay et al*., 2015] and auroral disturbances [*Davis*, 1971; *Wickwar &*

Carlson, 1999; *Nygren et al.*, 2015]. Some of the observed variability in the ionosphere is also due to the waves generated due to orography or seismic activity [*Wickwar & Carlson*, 1999; *Pulinets & Liu*, 2004].

Secondary gravity waves can be launched by dissipating GWs in the thermosphere [*Vadas & Liu*, 2009]. These secondary waves are produced at high altitudes and when they break in the lower thermosphere they may travel horizontally for many hundreds of kilometers, potentially triggering plasma instabilities widely known as Perkins instability [*Perkins,* 1973]. *Behnke* [1979] made observations using the Arecibo observatory and noted structures like height layer bands in the plasma associated with large electric fields which were attributed to Perkins instability [*Perkins*, 1973]. *Mathews and Harper* [1972] also observed midlatitude spread F with the Arecibo incoherent scatter radar and on one occasion they concluded that spread F occurred due to the tilts in the ionosphere caused by enhanced ionization traveling at the location.

Cosgrove and Tsunoda [2002b, 2004] show that the sporadic E and the F layers in the midlatitude ionosphere are electrodynamically coupled and the electric fields arise from the polarization of the sporadic E layer in turn causing the height bands in the plasma associated with the Perkins instability [*Kelley et al.*, 2003; *Tsunod*a 2006; *Cosgrove*, 2007; *Yokoyama et al.*, 2009]. Our previous study for Wallops Island [*Bhaneja,* 2009] showed the occurrence of more spread F when the angle between the dusk terminator and local magnetic field (declination angle) was minimum indicating that efficient electric field mapping between conjugate hemispheres is important for the occurrence of spread F. Different large-scale vertical electric fields are also created by thunderstorms and orography [*Pulinets & Liu*, 2004]. The lightning induced phenomenon such as red sprites and blue jets create the anomalous electric field coupling to the ionosphere [*Lastovicka*, 2006].

Midlatitude spread-F is a night time phenomenon observed mainly using the ionosondes [*Bowman*, 1990, 1994; *Kelley*, 2003, *Bhaneja et al.*, 2009, *Earle et al.*, 2010] where the irregularities are observed on the ionograms which are plots of frequency vs. height obtained by reflections of the transmitted signal into the ionosphere when they match the plasma frequency

[*Bhaneja et al.*, 2009]. An ionosonde consists of a radio transmitter and a series of receivers that is capable of inferring atmospheric electron density variations through the transmission and reflection of radio waves in the ionosphere. The transmitted radio waves penetrate the plasma layer until the plasma is dense enough to reflect them; this occurs when the wave frequency matches the plasma frequency. The measurements taken include the reflected signal frequency, and the time between transmission and reception of the signal. The intensity of these reflected signals is graphically depicted as a function of frequency and virtual height to produce ionograms. Virtual height is defined as the product of the speed of light in vacuum and the total transit time of the reflected signal, divided by two.

Figure 1 shows two ionograms indicating different conditions of the ionosphere. 1.1 indicates a quiet ionosphere, represented by a single trace. A uniform ionospheric layer produces a smoothly varying response corresponding to the normal increase in plasma density/frequency versus altitude. In contrast, density corrugations in the ionosphere create multiple reflections over the footprint of the incident signal in the ionosphere, leading to multipath and a subsequent spreading of the measured response either in frequency (frequency spread F), height (range spread F), or both. 1.2 indicates a disturbed ionosphere, represented by multiple traces and/or unusually thick traces in the ionogram. Note that there is a second trace or hop visible in both the ionograms, which is due to double reflection of the pulse (from the ionosphere to the ground, back to the ionosphere and back to the receiver). These second hop traces contain no additional information, and are ignored in the analysis of the ionograms. *Bowman* [1981] originally suggested that gravity waves could cause such plasma density distortions in the ionosphere, which would be manifested as midlatitude spread F in ionograms. This hypothesis was empirically confirmed by simultaneous *in-situ* and remote observations, as reported by *Earle et al.* [2010].

The spread F in the ionogram is historically classified into two types: range and frequency spread F. Range spread F refers to a condition in which there are multiple echoes at different ranges for each frequency. Frequency spread F is the case in which there are multiple echoes at different frequencies around the critical frequency for same height. Range and frequency spreading can occur simultaneously (as they are in the right panel in Figure 1) or separately.

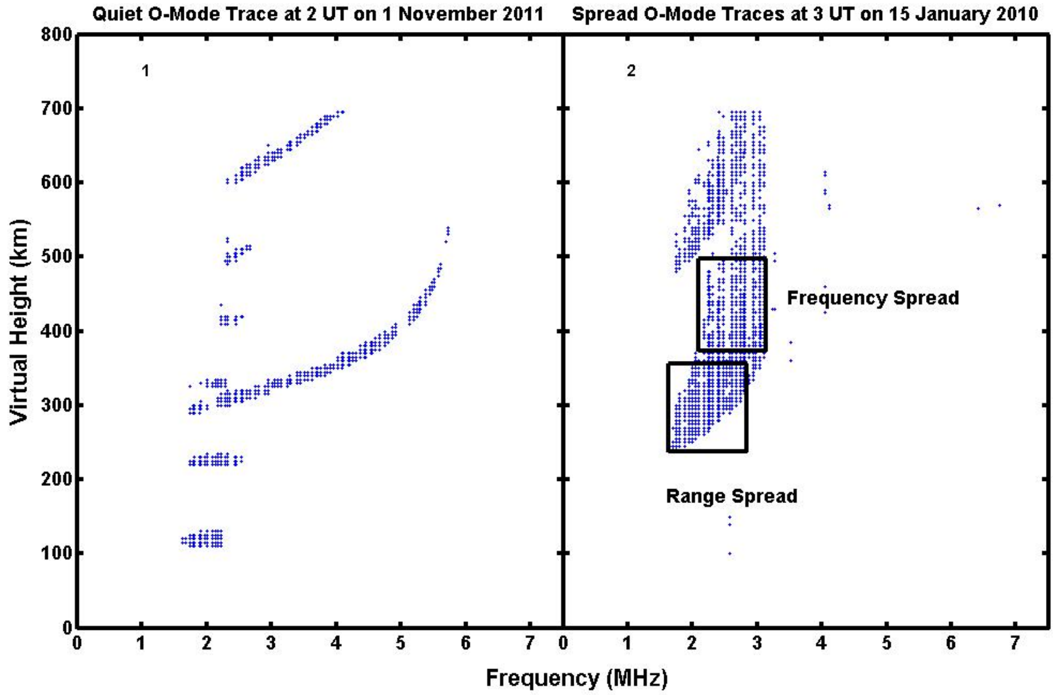

FIGURE 1 – 1. Midlatitude Non-Spread F event on 1 November 2011 at 2 UT. 2. Midlatitude Spread F event on 15 January 2010 at 3 UT.

Bhaneja et al., [2009] studied midlatitude spread F (MSF) at Wallops Island and determined its seasonal and solar cycle variation over an entire solar cycle (1996-2006) and discovered an interesting variation of MSF with the declination angle in that study. Here we are extending that study to about sixteen years (1996-2011) and including four more North-American sites at different longitudes from 67.1°W to 120.5°W with different declination angles from -14° to 13° to study the gross features of seasonal, solar cycle and longitudinal variations of MSF. This allows us to look and compare the variation of MSF with solar cycle and also with season for five different American sector sites having different local geographic features; Puerto Rico in the Caribbean, Wallops island on the east coast, Dyess in the southern plains, Boulder in the rocky mountains and Vandenberg on the west coast. The widely varying locations and geographic features at these sites enable an interesting look into the seasonal variation of MSF. We also look at the relationship between MSF and the angle of the terminator relative to the geomagnetic field (varying from -14° to 13° for the sites in this study) to see if the temporal variation in field-aligned conductivity is correlated with MSF observations, as it appeared to be for Wallops Island in our earlier study [*Bhaneja et al.,* 2009]. We use the previously established pattern recognition algorithm from this paper with some modifications to automatically detect midlatitude spread F in ionograms from the five different stations to investigate the variations in range and frequency spread F with particular emphasis on how these variations correlate with season and solar cycle at each ionosonde station.

We discuss the ionosonde database and the algorithms used to objectively and automatically identify MSF events in section 2. The statistical results for the five stations are presented in section 3 while section 4 discusses how these results vary versus solar cycle and season and their correlation with geomagnetic influence. Section 5 summarizes the conclusions and suggests possible future paths of inquiry.

2. Data Presentation

The data used in this study have been obtained from digisondes placed at 5 North American midlatitude sites: Ramey AFB, Puerto Rico (18.5°N, 67.1°W, -14° declination angle), Wallops Island, Virginia (37.95°N, 75.5°W, -11° declination angle), Dyess, Texas (32.4°N, 99.8°W, 6.9° declination angle), Boulder, Colorado (40°N, 105.3°W, 10° declination angle), and Vandenberg AFB, California (34.8°N,120.5°W, 13° declination angle). Figure 2 shows the five stations on the map of North-America. Previous studies on MSF have been conducted using ionosondes, but this study utilizes a more advanced instrument known as a digisonde [*Bhaneja et al.,* 2009, *Bowman* 1994 and references therein]. The digisonde is essentially the advanced digital version of the standard continuous-wave ionosonde technique [*Bibl & Reinisch*, 1978], This instrument measures the parameters required to characterize the reflected wave: amplitude, phase, and frequency, for both the ordinary (O) and extraordinary (X) component of the reflected waves [*Rishbeth & Davis* 2001*; Bibl & Reinisch* 1978].

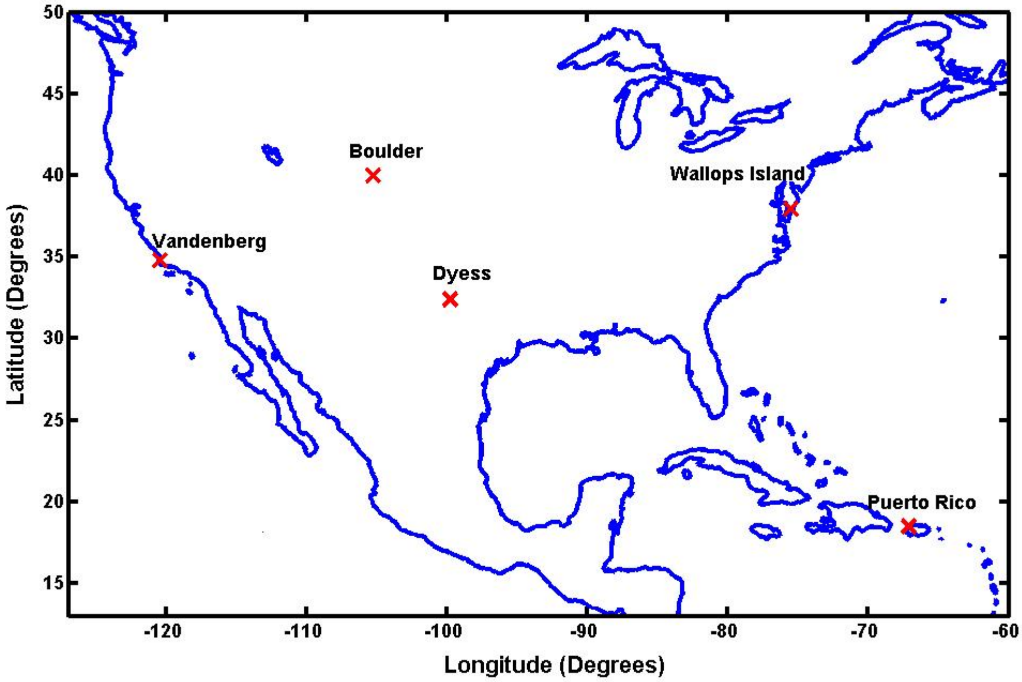

FIGURE 2- Map showing the location of the five different midlatitude stations across North-America that are used in this study.

2.1 Data Analysis – methodology

Sixteen years (1996-2011) of data have been analyzed from the digital ionosondes (digisondes) in Puerto Rico, Wallops Island, Dyess and Vandenberg. Eight years (2004-2011) years of data are available from the Boulder digisonde. Midlatitude spread F is a nighttime phenomenon and thus the data for nighttime between 7 PM -6 AM LT (0-10 UT varying with different time zones) are processed to identify spread conditions.

Raw digisonde data are filtered and processed to generate ionograms for statistical analysis in the following manner. First the raw data are converted to a human readable text format using an algorithm developed by Dr. T. Bullett and run through a noise threshold algorithm to remove data that are questionable due to low signal to noise ratios. The remaining data are processed using an edge detection and a pattern recognition algorithm designed to identify the two types of MSF (see *Bhaneja et al.*, 2009) and has been explained here. O-mode data are used exclusively for this analysis, since this mode is insensitive to the local magnetic field intensity. Thus O-mode data can be analyzed without a need for sophisticated magnetic field models.

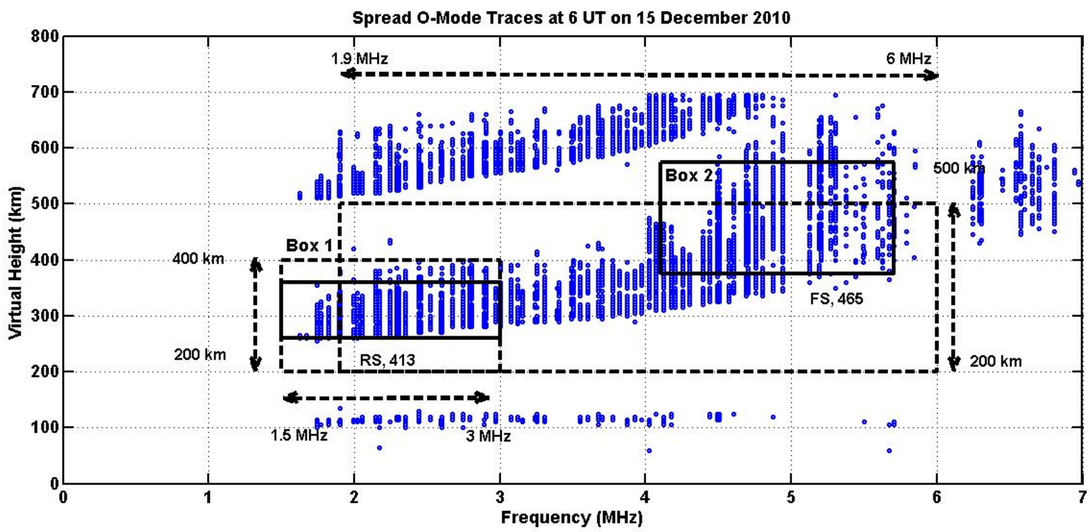

FIGURE 3 – An ionogram showing boxes (solid lines) drawn indicating range (RS) and frequency (FS) spread F for box 1 and box 2 respectively. The numbers beside the RS and FS indicate the pixel count inside the two boxes. The dashed box shows boundary conditions for night time spread F.

Figure 3 shows both range and frequency spread F identified by box 1 and box 2 (solid lines) respectively. To avoid human bias and analyze the large number of ionograms used in this study it is necessary to create autonomous algorithms for identifying spread F conditions. Figure 3 illustrates this process, using the total pixel count in each box to determine the presence of spread F conditions. The locations of the two boxes vary for each ionogram and are determined using edge detection. In essence the algorithm determines the right and the bottom edges of boxes 1 and 2 respectively. The box 1 boundary limits for the edge detection are constrained to lie between 200-400 km and 1.5-3 MHz (dashed box). The bottom edge for box 1 is determined by counting the pixels for each altitude starting at 200 km; when the pixel count exceeds 6 the corresponding altitude is chosen as the bottom edge of box 1. The height of this box is fixed at 100 km. Similarly for box 2, the box boundary limits are set to 200-500 km and 1.9-6 MHz (dashed box). Also for box 2, for the spring to fall months from day 80 till day 300 for 0-1 UT, the box limits are 3.5-11 MHz, and for 2-10 UT it stays as 1.9-6 MHz. The right edge for box 2 is determined by counting the pixels for each frequency starting at 6 MHz and proceeding to lower frequencies. When the pixel count exceeds 6, the corresponding frequency is chosen as the right edge of box 2. The width of this box is varied by the edge. If the right edge is determined to be greater than 5 MHz, the box width is 1.6 MHz, if the edge is between 3.2-5 MHz, the width is 1 MHz, and less than 3.2, the width is 0.5 MHz. We then take the altitude of the frequency determined using edge detection. If the altitude is up to and equal to 300 km, the minimum and maximum height are taken as 10 km and 200 km respectively. If the altitude is between 300-400 km, the minimum and maximum height are taken as 25 km and 175 km respectively. If the altitude is greater than 400 km the minimum and maximum height are 50 km and 150 km respectively. The final height of the box is then taken as the altitude minus the minimum height to the altitude plus the maximum height. For example, in Figure 3, the edge detection gave frequency as 5.7025 MHz at 400 km; the box 2 width was then 1.6 MHz, (5.7025 minus 1.6 gives us 4.1), which made the box position from 4.1-5.7 MHz. The box 2 height was from altitude of 400 km minus the minimum height of 25 km and altitude of 400 km plus the maximum height of 175 km making our box 2 position from 375-575 km. These conditions for box 2 were set so as to reduce any overlap with the range spread in box 1. The limits on the two boxes have been chosen to cover night-time spread F while being careful not to include sporadic E and second hop traces.

Once the pixels are counted they are compared against a set threshold to determine spread F condition. These pixel counts are shown in the Figure 3 with RS and FS for range and frequency spread F for the two boxes. The thresholds are determined by randomly choosing a set of ionograms and determining the threshold counts for spread/non-spread conditions. These autonomous edge detection and pixel counting algorithms have been extensively debugged by spot-check comparisons with human perceptions for a wide variety of cases and conditions and these were found to be true for every single case. The goal of the algorithm is to identify range and frequency spread F without human biases and false positives. The statistics generated from this autonomous spread F identification process should therefore be in excellent agreement with those using a “man-in-the-loop” judgment.

As spread F is a night time phenomenon, only data between 7 PM-6 AM local time are considered in this study. The digisondes used in this study operate continuously and produce ionograms at 15 minute intervals providing us with 44 ionograms/night for our study. A spread event is cataloged if continuity in spread ionograms is observed with no interruption of more than thirty minutes (two consecutive ionograms). If more than one event is observed for a night, only the longer event is recorded. If two events of equal length are observed, only first event is saved for further analysis. This approach has been justified and explained in *Bhaneja et al.* [2009].

Once a spread F event has been identified by the automated algorithm, the onset time, duration and type of spread F event are recorded and archived. This process is systematically applied to the data from all five stations. Using this very large MSF event database, statistical results are plotted to reveal the seasonal and solar cycle patterns for MSF. Some representative results for December 2009 at Wallops Island are shown in Figure 4. Statistics of this type for all five stations over all of solar cycle 23 (1996-2008) and the beginning of cycle 24 (2009-2011) were made and studied. Note that the station at Boulder only came online in 2004, and therefore a complete solar cycle is not available for this station.

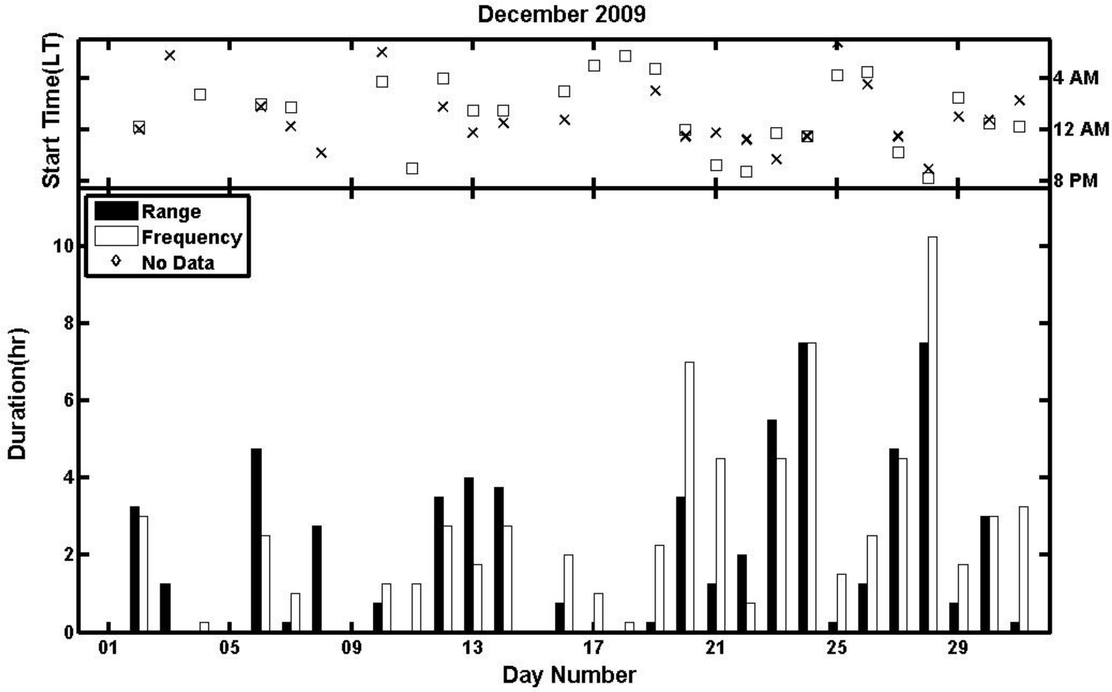

FIGURE 4 – Monthly occurrence plot for December 2009 showing range and frequency spread F onset time and duration for night time hours between 8PM-6AM LT. Black bars indicate range spread F and white bars indicate frequency spread F. The cross symbol denotes the start time for range spread F and the square symbol denotes the start time for frequency spread F.

2.2 Statistical Results

Automated processing as described above has been performed for the entire data set. Figures 5 and 6 show the solar variation for both types of MSF for all the stations. Figures 7 and 8 show the seasonal variations of MSF. Figure 9 provides another contribution towards the seasonal variation with the declination angle. Figure 10 shows the variation of MSF with geomagnetic and solar activity.

2.2.1 Solar cycle variation

Figure 5 shows the number of spread days for each year between 1996-2011 for the 5 sites. The top panel shows the solar flux between 1996-2011, and the other 5 panels have stations in order of increasing declination angle: Puerto Rico, Wallops Island, Dyess, Boulder and Vandenberg. The left and right axes represent the number of spread days and percentage of data available, respectively. Black bars represent range spread F while white bars represent frequency spread F. The diamond symbols represent percentage of data available. There are no data available for the Boulder ionosonde prior to 2004. Most of the MSF events are observed during the solar minimum years (1996-1999 and 2005-2009), and this is consistently observed for all five sites.

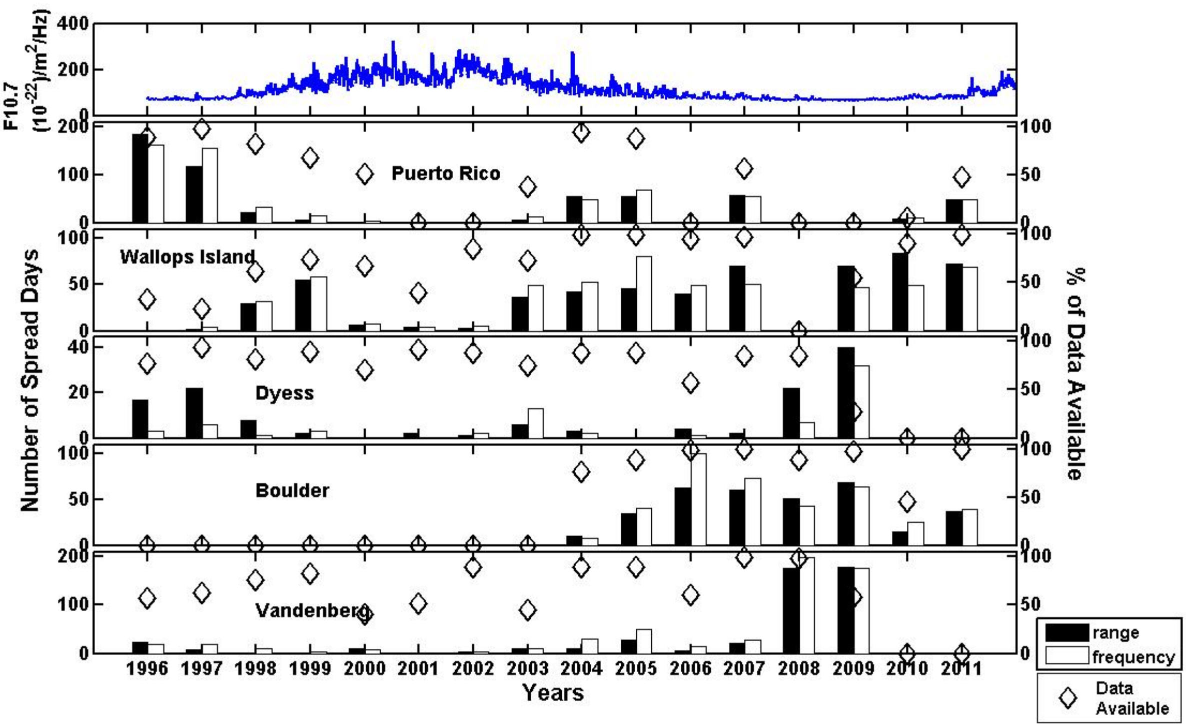

FIGURE 5 – Plots show the solar cycle variation of spread F for 16 years (1996-2011) of data for Wallops Island, Dyess, Vandenberg and Puerto Rico and 7 years (2004-2011) of data for Boulder. The top panel shows the solar flux data which is higher during the solar maximum years (2000-2002). The left-hand axis represents the number of spread days and the right-hand axis displays the percentage of data available. The black bars represent range spread F while the white bars represent frequency spread F. The diamond symbols represent percentage of data available. The MSF events are more during solar minimum than solar maximum.

Figure 6 shows the average duration of spread days for each year between 1996-2011 for the 5 sites. This figure is similar in format to Figure 5, with the top panel showing solar flux and the rest of the panels representing stations in order of decreasing longitude. The left and right hand side axes represent the average duration of spread days and the percentage of data available, respectively. The total number of hours for the longest duration spread F event on each night is averaged for each year. The average duration of MSF events observed in each year is longer during the solar minimum years (1996-1999 and 2005-2009), and this is consistently observed for all five sites.

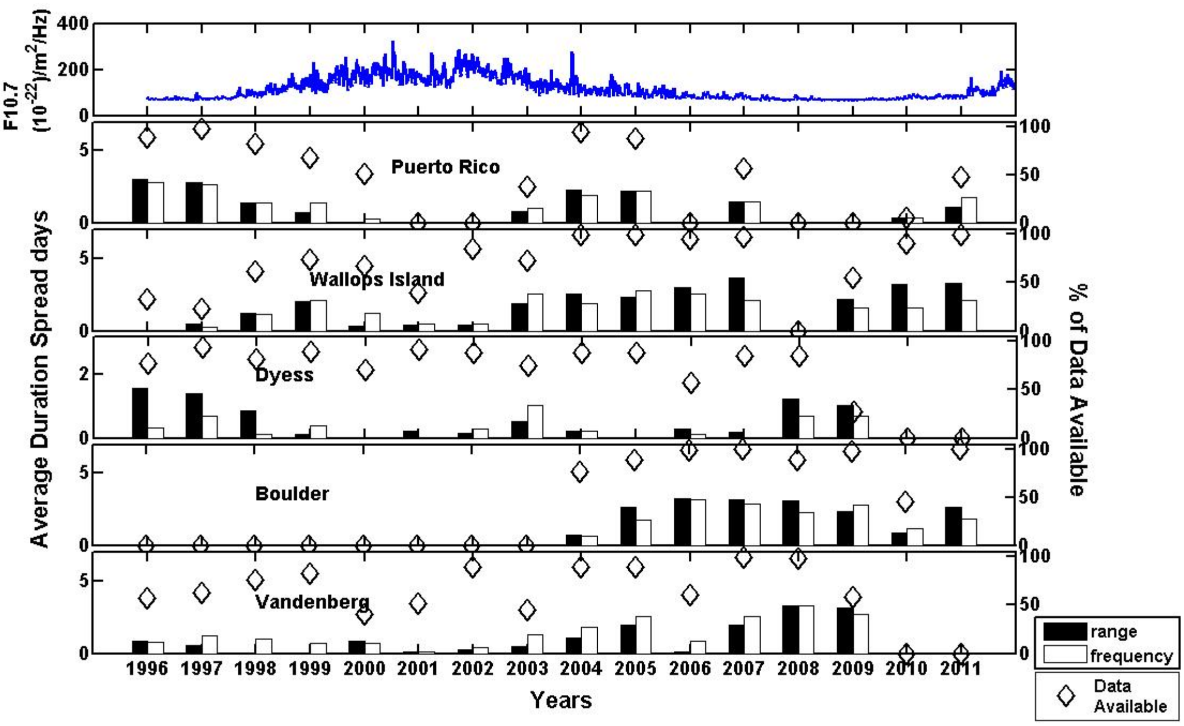

FIGURE 6 – Plots shows the solar cycle variation of spread F for more than 15 years (1996-2011) of data for Wallops Island, Dyess, Vandenberg and Puerto Rico and 7 years (2004-2011) of data for Boulder. The top panel shows the solar flux data which is higher during the solar maximum years (2000-2001). The left-hand axis represents the average duration of spread days and the right-hand axis displays the percentage of data available. The black bars represent range spread F while the white bars represent frequency spread F. The

diamond symbols represent percentage of data available. The MSF events have longer duration during solar minimum than solar maximum.

2.2.2 Seasonal variation

Figure 7 shows the average number of spread days per month for a given year. The average is calculated by first obtaining the sum of spread F nights for each month for each available year. These sums for each year are divided by the number of available years of data to obtain the averages. Black bars represent range spread F while white bars represent frequency spread F. The diamond symbols represent the numbers of years of data available for each month. MSF is common during the months of December and January but vary differently during the other months for all the sites. All the stations show different seasonal variations for MSF, presumably due to their varying longitudes.

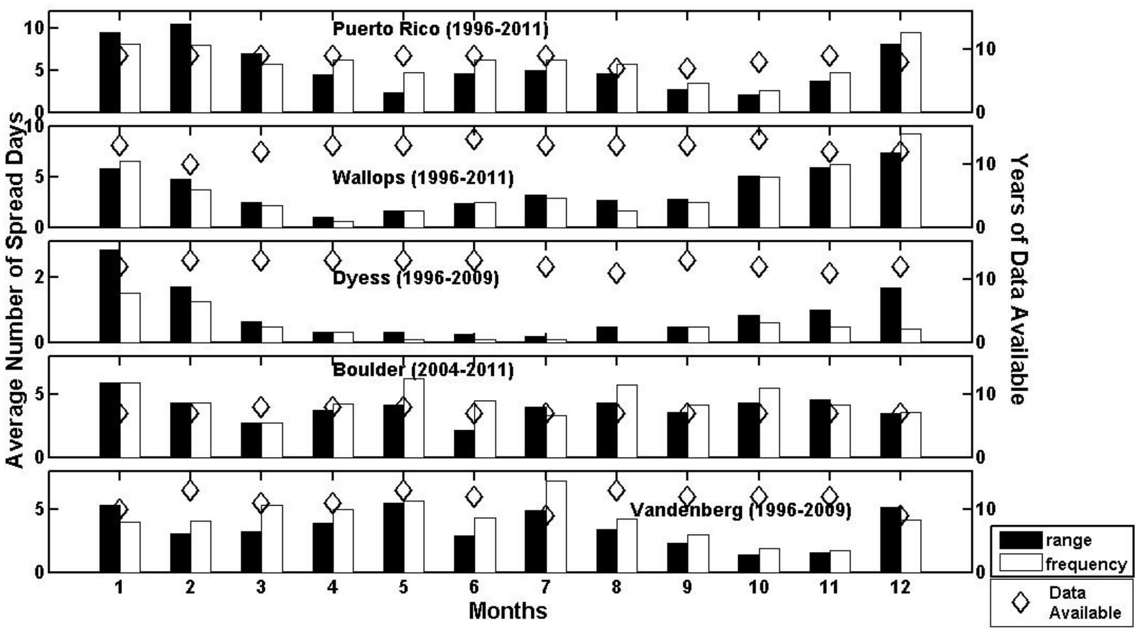

FIGURE 7 – Plots shows the seasonal variation of spread F. The data have been plot for each month for more than 15 years (1996-2011) of data for Wallops Island, Dyess, Vandenberg and Puerto Rico and 7 years (2004-2011) of data for Boulder. The left-hand axis represents the average number of spread days and the right-hand axis displays the

years of months of data available. The black bars represent range spread F while the white bars represent frequency spread F. The diamond symbols represent data available. All the sites show varying seasonal variation of MSF. MSF is common during the months of December and January but vary differently during the other months for all the sites. There is clearly a seasonal dependence on various factors such as the different longitudes, declination angles, terrestrial weather systems, and orography.

Figure 8 shows the average duration of spread days per month averaged for all the available years. The total number of spread F hours for the longest duration events on each night are accumulated each month and then divided by the total number of spread F nights. These monthly averages are then divided by the number of available years of data to obtain the averages. The duration of the MSF for the different stations also show different seasonal variations, presumably due to their varying longitudes.

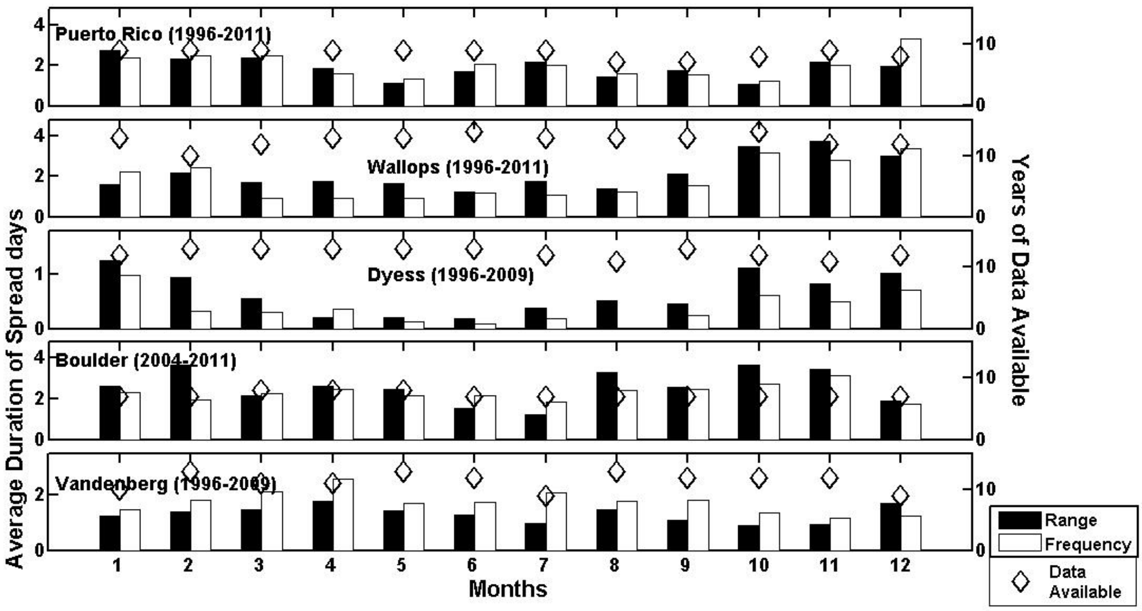

FIGURE 8 – Plots shows the seasonal variation of spread F. The data have been plotted for each month for more than 15 years (1996-2011) of data for Wallops Island, Dyess, Vandenberg and Puerto Rico and 7 years (2004-2011) of data for Boulder. The left-hand axis displays the average duration of spread days and the right-hand axis displays the years of months of data available. The black bars represent range spread F while the white bars

represent frequency spread F. The diamond symbols represent data available. All the sites show varying seasonal variation of MSF. There is clearly a seasonal dependence on various factors such as the different longitudes, declination angles, terrestrial weather systems, and orography.

Figure 9 shows the average number of spread F days per month for a given year plotted along with the angle between the declination angle and the terminator (represented by the black line). The angle variation is plotted with the spread F to compare its variation around the seasons.

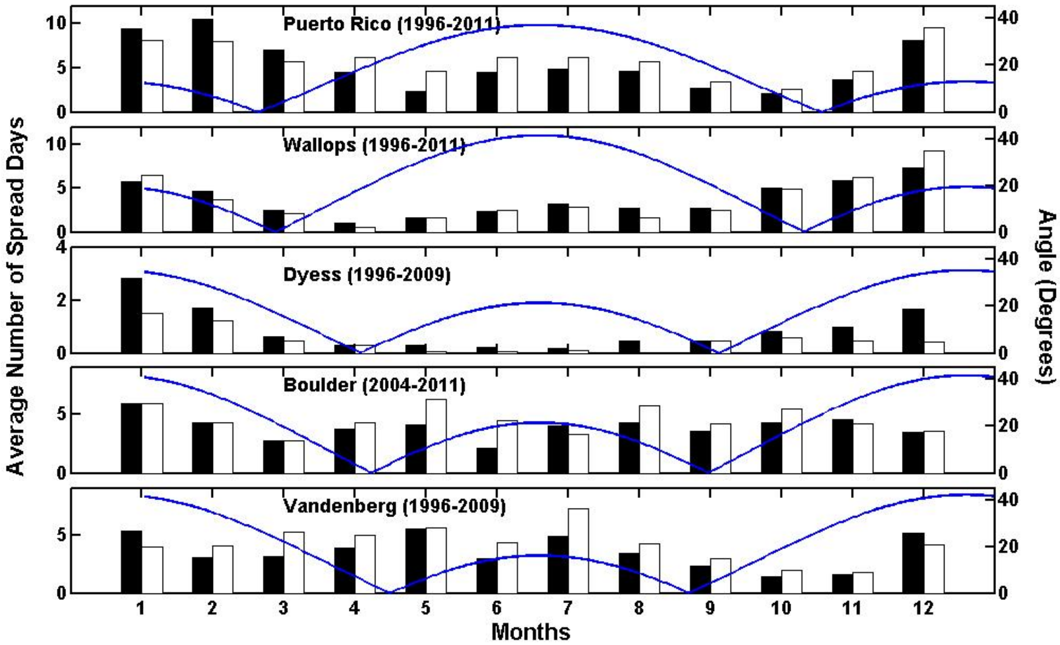

FIGURE 9 – Plots show the seasonal variation of range and frequency spread F of the different sites having different magnetic declinations from -14, -11, 6.9, 10 and 13 degrees. The left-hand axis displays the average number of spread days and the right-hand axis displays the angle in degrees. The black bars represent range spread F while the white bars represent frequency spread F. The line represents the angle between the dusk terminator and the local magnetic field. The spread F varies with the different locations. Puerto Rico, Wallops, and Vandenberg seem to have more spread events for the lower declination angles; this holds more for Wallops Island, than for Puerto Rico and Vandenberg. Also, there is

more spread F during winter for Wallops and Dyess, while there is more during spring and summer for Boulder and Vandenberg.

Figures 5-9 show that both the occurrence probability and the duration of MSF events have varying seasonal and solar cycle patterns that are different for each of the five sites. This suggests that geographical locations, orographic features, and/or local weather patterns may be important factors in the characteristics of gravity waves that propagate to ionospheric altitudes, and on their effects on the ionosphere.

2.2.3 Geomagnetic variation

Figure 10 shows both the duration of range (top panel) and frequency (bottom panel) spread F events versus the F10.7. The average duration for the five stations for the corresponding years is taken and plotted. The solar minimum (1996-1998, 2003-2010) years are shown as filled circles while solar maximum (1999-2002, 2011) years are shown as squares. Most long duration events for both range and frequency spread F occur during the solar minimum years. Few longer duration events occur during solar maximum years.

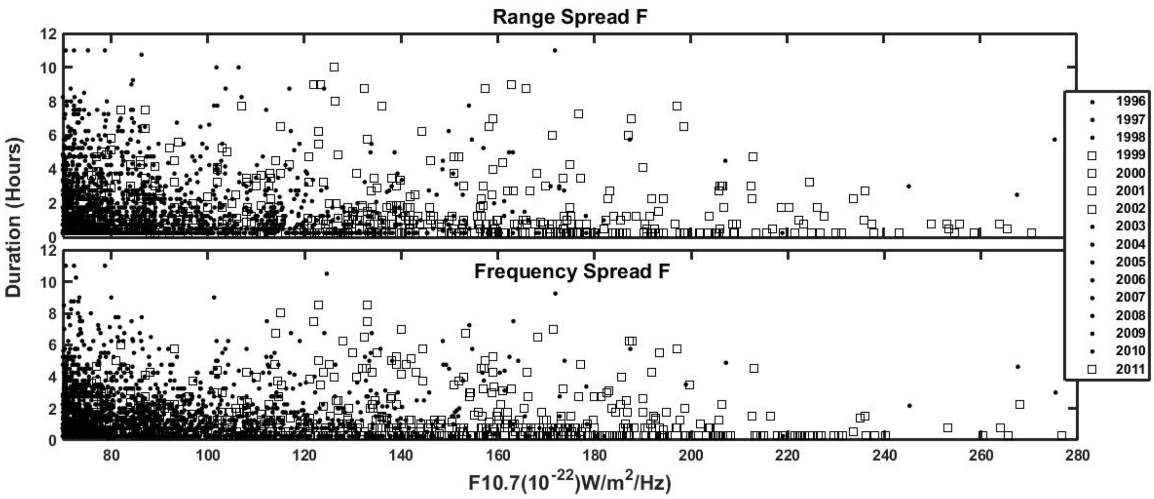

FIGURE 10 – Plots show the average duration of range and frequency spread F events for the five stations versus F10.7. The solar minimum (1996-1998, 2003-2010) years are shown as filled circles while solar maximum (1999-2002, 2011) years are shown as squares.

Figure 11 shows the number of range spread F events for the corresponding kp values. For each spread F event, the maximum Kp value from the previous 12-hour periods are used. Due to the different spread F events corresponding to different kp values for each station, we have made the plots for separate stations. The solar minimum (1996-1998, 2003-2010) years are shown as filled circles while solar maximum (1999-2002, 2011) years are shown as squares. Most of the spread F events occur during low kp values below 5 and very few occur for high kp values.

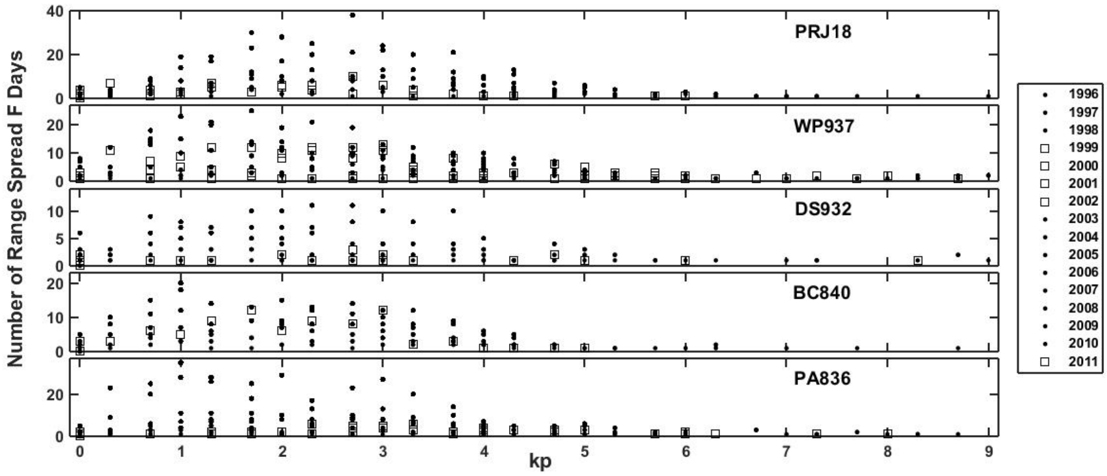

FIGURE 11 – Plot show the geomagnetic variation of range spread F. The number of range spread F events versus kp values for all the stations. The solar minimum (1996-1998, 2003-2010) years are shown as filled circles while solar maximum (1999-2002, 2011) years are shown as squares. Most spread F events are for lower kp values.

3. Discussion

The data presented here indicate that the occurrence rate and duration of midlatitude spread F are higher during solar minimum than during solar maximum as is evident from Figures 5 and 6. It can be seen from the plots that this statement applies for all five North-American stations. During 1996-1999 and 2004-2010, which are the solar minimum years, there are significantly more spread F events, and their duration is longer than in the solar maximum period. During the solar maximum in 2000-2003 (indicated by the higher solar flux values during those years), there are fewer events of shorter duration. *Bowman* [1992] similarly shows higher occurrence of MSF for solar minimum then solar maximum using data from Australia. This pattern suggests that lower thermospheric temperatures and neutral densities are conditions that may enable the physical processes that lead to MSF. Gravity waves are considered to be the primary source of MSF and these waves tend to have larger amplitudes at a given altitude during solar minimum than during solar maximum when they propagate to higher altitudes [*Vadas*, 2007]. Thus, it can be inferred from its solar cycle dependence that the amplitudes of gravity waves in the lower thermosphere may be a key factor in generating MSF.

Martinis et al. [2010] showed an anti-correlation between medium scale TIDs and solar activity using imaging data at Arecibo. *Candido* [2008] discussed similar results for Brazil, stating that most of the observable medium scale TIDs occur during low solar activity as compared with high solar activity. TIDs are plasma manifestations of atmospheric gravity waves propagating in the thermosphere [*Kotake et al.,* 2007]. Solar cycle 23-24 had an unusually long solar minimum and had reportedly the lowest thermospheric densities ever recorded [*Emmert et al*., 2010] as well as an extended contracted ionosphere [*Klenzing et al.,* 2011], so it is not surprising that the occurrence rates for MSF in the North-American sector maximize in this period. Figure 5 shows the highest number of spread F days during 2008-2009 for Wallops, Dyess, Boulder and Vandenberg. There are no data available for Puerto Rico for those two years, but Puerto Rico shows a similar pattern for the previous solar minimum during 1996-1997. Another interesting observation evident in Figure 5 is that most stations experience more range spread F events during solar minimum, and more frequency spread F events during solar maximum. This pattern has also been reported by *Abdu et al.* [1983] over Fortaleza, Brazil and also by *Candido et al.* [2011] over Cachoeira Paulista, Brazil.

The seasonal variation is particularly interesting, since this has not been thoroughly studied. Figures 7-9 show the seasonal variation of the MSF for all five stations; all the stations show different seasonal variations, presumably due to their varying longitudes, declinations, or localized forcing from lower altitude sources. The observations are summarized in Table 1. The seasonal variation provides a longitudinal variation of spread F, and each station has MSF during different seasons; in Ramey, Puerto Rico during winter, in Wallops Island, Virginia during vernal equinox and winter, in Dyess, Texas during winter solstice, in Boulder, Colorado during early summer and autumn equinox and in Vandenberg, California during summer and winter solstice. These figures also indicate that MSF is common at all latitudes in this study during the months of December and January. This coincides with the general notion of the occurrence of medium scale gravity waves for the north-American region during the winter solstice [*Martinis et al*., 2010]. The seasonal dependence of MSF at Puerto Rico is similar to previously published statistics of MSTIDs observed at Arecibo [*Martinis et al,* 2010]. Another observation is that the MSF occurs the least during spring equinox for all the sites except for Vandenberg and being all the way on the west coast may have some contribution towards this occurrence or non-occurrence factor.

Stations	**Latitude**	**Longitude**	**Declination**	**Season with maximum MSF occurrences**	**Season with minimum MSF occurrences**
Ramey, Puerto Rico	18.5°	67.1°	-14°	Winter solstice	Spring equinox, Vernal equinox
Wallops Island, Virginia	37.95°	74.5°	-11°	Vernal equinox, winter solstice	Spring equinox, Summer
Dyess, Texas	32.4°	99.8°	6.9°	Winter solstice	Spring, Summer, Vernal Equinox
Boulder, Colorado	40°	105.3°	10°	Early summer, autumn equinox	Spring Equinox, Winter
Vandenberg, California	34.8°	120.5°	13°	Summer solstice, winter solstice	Fall

TABLE 1-Summary of seasonal variation of MSF

Another interesting feature of the data, shown in Figure 9, is the variation of MSF with the angle of declination. The data from different stations Puerto Rico, Wallops Island, Dyess, Boulder and Vandenberg with declination angles -14°, -11°, 6.9°, 10° and 13° respectively are plotted. Out of the five stations, three, viz. Puerto Rico, Wallops, and Vandenberg seem to have more spread events for the lower declination angles; this holds more for Wallops Island, than for

Puerto Rico and Vandenberg. Also, there is more spread F during winter for Wallops and Dyess while there is more spread F during spring and summer for Boulder and Vandenberg, which is yet another variation with the different declination angles. The varying dip angles which are 46.4°, 66.2°, 61.3°, 67° and 59.3° for Puerto Rico, Wallops Island, Dyess, Boulder and Vandenberg respectively do not show any significant effect in the statistics. Wallops and Boulder have similar dip angles as do Dyess and Vandenberg, but with different spread patterns. The Perkins instability growth rate is inversely proportional to the dip angle, making it decrease with the increase in the dip angle, but there is no such pattern observed with our data.

The occurrence of more spread F when the angle between the dusk terminator and local magnetic field is minimum indicates that efficient electric field mapping between conjugate hemispheres is important for the occurrence of spread F. The process of E-fields mapping along the magnetic flux tube is more efficient when both ends of the tube experience sunset at roughly the same time. The reduced conductivity along the entire flux tube would lead to better E-field mapping because the fields would not drive currents in the E-regions of either hemisphere, so the plasma motions perpendicular to B could be sustained for longer periods (the fields wouldn't be shorted out). Similar hypothesis for equatorial spread F has been proposed by *Tsunoda* [1985] and shown by *Aarons* [1993] for equatorial scintillation. *Abdu at al*., [1992] also talks about declination angle control over the sporadic E and F layers. A conjugate point equatorial experiment in Brazil conducted by *Abdu et al*., [2009] shows similar electrodynamical coupling during sunset hours giving rise to spread F conditions. Even though these were equatorial region studies, from our earlier Wallops Island study [*Bhaneja,* 2009], we conjectured that the alignment of the terminator and the flux tube might be an important factor in MSF generation. This new study includes more data from more geographically distributed sites, and it reveals that the terminator/flux tube alignment condition seems to hold for some stations (including Wallops Island, Puerto Rico and Vandenberg) but not for others. Thus, we are forced to conclude that the terminator/flux tube alignment condition may be a factor in MSF development, but it is not the only factor of significance, and is in fact not the dominant factor in MSF formation.

MSF can also vary due to solar effect and geomagnetic forcing as seen in Figures 10 and 11. Figure 10 shows that most long duration range and frequency spread F events occur during solar minimum (1996-1998 and 2003-2010) years. During the solar maximum (1999-2002, 2011) years, the events are shorter. There are a few longer events during solar maximum too, but most of them are short duration events. This observation is similar to what we see from Figures 5 and 6. Figure 11 shows the geomagnetic variation of MSF for all the different stations. The number of range spread F events occur more for low and moderate kp events while very few events occur for higher kp values. This also holds true for the solar minimum years which has more number of range spread F days for low kp values. It can be seen from the plots that this statement applies for all five North-American stations. The same pattern holds for frequency spread F and for the duration of both range and frequency spread F events. All the panels show that MSF is more prevalent during quiet times and during solar minimum.

The other major factor in MSF formation is the troposphere weather forcing; the prevalence and/or severity of thunderstorms, lightning, hurricanes, and tropical disturbances. The thunderstorms can also sometimes cause an increase in sporadic E and through that in the electron density in the F region [*Kazimirovsky*, 2002]. Presence of sporadic E events can also coincide with MSF events due to the electrodynamical coupling between the E and F regions [*Kelley et al*., 2003; *Haldoupis et al*., 2003; *Cosgrove*, 2007 and references therein]. We noticed this for Boulder where sporadic E is heavily observed and most of the times these events were coincident with MSF occurrences. The same goes for Puerto Rico being in lower latitudes also had more sporadic E events and some of them were coincident with massive spread F events. These terrestrial weather patterns vary with season that competes with or overcomes the declination and terminator alignment criterion. Another effect of thunderstorms is the manifestation of waves, mainly short -period gravity waves and these affect the F region [*Lay et al*., 2013, *Lay et al*., 2015]. These wave patterns are visible in the critical frequency and the electron density values. We conducted spectral analysis for some individual months and observed short-period wave signatures from 30 minutes to 4 hours in the foF2 values. But we need to analyze this deeply and also include weather data including lightning and storm data to find any correlations.

Another factor can be the surface features such as the orographic factors [*Pulinets & Liu*, 2004]. The Mountain ranges affect the motion of weather systems and produce lee waves that may have seasonal dependences affecting sites in different ways. This is of particular importance for the Boulder ionosonde which coincidentally also exhibits a lot of sporadic E events along with a disturbed second hop or reflection on the ionograms indicating a geographical impact on the observations. Coastal effects may also play a role. Puerto Rico is in the Caribbean, Wallops is an island on the east coast, Dyess is inland and Vandenberg is in the west coast.

Conclusion

This statistical study has established the seasonal and solar cycle variations of midlatitude spread F at five different North-American sites spanning the range between Puerto Rico and California. There are more and longer events during solar minimum years for all 5 stations. Increased MSF is detected at Dyess and Vandenberg during the extreme solar minimum years (2008-2009) relative to the previous solar minimum (1996-1997). The seasonal variation provides a longitudinal variation of spread F, and each station has maximum MSF occurrence during different seasons; winter in Puerto Rico, vernal equinox and winter in Virginia, winter solstice in Texas, early summer and autumn equinox in Colorado and summer and winter solstice periods in California. The minimum MSF happens during spring equinox for all the sites except for Vandenberg. Another interesting pattern is observed for Puerto Rico, Wallops, and Vandenberg: these three sites have more spread F when the angle between the magnetic field line and the terminator is minimum. This is an interesting observation as all these three sites have different declination angles, ranging from -14°, -11°, and 13° respectively. Also, there is more spread F during winter for Wallops and Dyess while there is more during spring and summer for Boulder and Vandenberg, which is yet another variation with the different declination angles. Declination angle alone is not enough to explain the occurrence of MSF however, since the relationship does not hold at all five sites. We must therefore conclude that while low conductivity along the entire flux tube may be important to MSF development, it is clearly not the dominant factor.

Further study needs to be conducted to determine the reason behind the observed seasonal pattern. Some stations seem to show the MSF due to possible electrodynamical coupling, others show a clear discrepancy, indicating that there might be other physical factors contributing or suppressing the conditions responsible for spread F. Geomagnetic variations have a very weak influence on MSF and this holds for each individual station in this study. To determine if the seasonal variation is due to tropospheric and orographic influences, further study should be conducted that uses weather conditions prior to each event. This may be achieved by using weather satellite images or other meteorological data. The past solar cycle is an ideal time period for such a study, since it was so long and so quiet geomagnetically. We intend to extend our work by creating a model to look at these factors and their impacts on MSF wherein we will possibly include more stations. Constructing and validating an empirical model is a significant task and is the next step. Having a model that can predict average behavior of mid-latitude spread F will hopefully be a great contribution to space science.

Acknowledgements. The data for this research was obtained from National Geophysical Data center, NGDC/NOAA at Boulder, Colorado. Preeti Bhaneja also thanks Dr. Jeff Klenzing for his invaluable help and advice and Dr. Patrick Roddy for editing help.

References

1. Aarons, J., The longitudinal morphology of equatorial F-layer irregularities relevant to their occurrence, *Space Science Reviews*, 63, 209-243, 1993.
2. Abdu, M. A., deMedeiros, R.T., and Nakamura, Y., Latitudinal and magnetic flux tube extension of the equatorial spread F irregularities, *J. Geophys. Res.*, *88(*A6*),* 4861–4868, doi:10.1029/JA088iA06p04861, 1983.
3. Abdu, M. A., Batista, I.S., and Sobral, J.H.A., A new aspect of magnetic declination control of equatorial spread F and F region dynamo, *J. Geophys. Res*., 97(A10), 14897–14904, doi:10.1029/92JA00826, 1992.

4. Abdu, M. A., Batista, I.S., Reinisch, B.W., de Souza, J.R., Sobral, J.H.A., Pedersen, T.R., Medeiros, A.F., Schuch, N.J., de Paula, E.R., and Groves, K.M., Conjugate Point Equatorial Experiment (COPEX) campaign in Brazil: Electrodynamics highlights on spread F development conditions and day-to-day variability, *J. Geophys. Res*., 114, A04308, doi:10.1029/2008JA013749, 2009.
5. Behnke, R., F layer height bands in the nocturnal ionosphere over Arecibo, *J.Geophys. Res*., 84, 974, 1979.
6. Bhaneja, P., Earle, G.D., Bishop, R.L., Bullett, T.W., Mabie, J., Redmon, R., A statistical study of midlatitude spread F at Wallops Island, Virginia, *J. Geophys. Res.,* 114, A04301, doi:10.1029/2008JA013212, 2009.
7. Bibl, K., and Reinisch, B.W., The universal digital ionosonde, *Radio Science*, 13(3), 519-530, 1978.
8. Boska, J., and Sauli, P., Observations of gravity waves of meteorological origin in the F-region ionosphere, *Phys. Chem. Earth*, 26, 6, 425-428, 2001.
9. Bowman, G.G., The nature of ionospheric spread-F irregularities in mid-latitude regions, *J. Atmosphere and Solar-Terrestrial Phys*., 43, 65-79, 1981.
10. Bowman, G.G., A review of some recent work on mid-latitude spread-F occurrence as detected by ionosondes, *J.Geomag.Geoelectr*., 42, 109, 1990.
11. Bowman, G.G., Upper-atmosphere neutral-particle density variations compared with spread-F occurrence rates at locations around the world, *Ann. Geophys*., 10, 676, 1992.
12. Bowman, G.G., Short-Term Delays in the Occurrence of Mid-Latitude Ionospheric Disturbances Following Other Geophysical and Solar Events, *J.Geomag. Geoelectr*., 46, 297 309, 1994.
13. Candido, C., Pimenta, A., Bittencourt, J.A., and Becker-Guedes, F., Statistical analysis of the occurrence of medium-scale traveling ionospheric disturbances over Brazilian low latitudes using OI 630.0 nm emission all-sky images, *Geophys. Res. Lett.,* 35, L17105, doi:10.1029/2008GL035043, 2008.
14. Candido, C.M.N., Batista, I.S., Becker-Guedes, F., Abdu, M.A., Sobral, J.H.A., and Takahashi, H., Spread F occurrence over a southern anomaly crest location in Brazil during

June solstice of solar minimum activity, *J. Geophys. Res*., 116, A06316, doi:10.1029/2010JA016374, 2011.

15. Cosgrove, R. B., and Tsunoda, R.T., A direction-dependent instability of sporadic E layers in the nighttime midlatitude ionosphere, Geophys. Res. Lett., 29(18), 1864, doi:10.1029/2002GL014669, 2002b.
16. Cosgrove, R.B., and Tsunoda, R.T., Instability of the E-F coupled nighttime midlatitude ionosphere, *J. Geophys. Res*., 109, A04305, doi:10.1029/2003JA010243, 2004.
17. Cosgrove, R. B., Generation of mesoscale F layer structure and electric fields by the combined Perkins and Es layer instabilities, in simulations, *Ann. Geophys*., 25, 1579, 2007.
18. Davis, M.J., On polar substorms as the source of large-scale traveling ionospheric disturbances, *J.Geophys. Res*., 76, 4525, 1971.
19. Earle, G. D., Bhaneja, P., Roddy, P.A., C. M. Swenson, C.M., Barjatya, A., Bishop, R.L., Bullett, T.W., Crowley, G., Redmon, R., Groves, K., Cosgrove, R., Sharon L. Vadas, A comprehensive rocket and radar study of midlatitude spread *F, J. Geophys. Res.*, 115*, A12339, doi:*10.1029/2010JA015503, 2010.
20. Emmert, J.T., Lean, J.L., and Picone, J.M., Recod-low thermospheric density during the 2008 solar minimum, *Geophys. Res. Letters*, 37, L12102, doi:10.1029/2010GL043671, 2010.
21. Haldoupis, C., Kelley, M.C., Hussey, G.C., and Sergei Shalimov, S., Role of unstable sporadic-E layers in the generation of midlatitude spread F, *J. Geophys. Res*., 108, A12, 1446, doi:10.1029/2003JA009956, 2003.
22. Hines, C.O., Internal atmospheric gravity waves at ionospheric heights, *Can. J. Phys*., 38, 1441–1480, 1960.
23. Kelley, M.C., and Fukao, S, Turbulent Upwelling of the Mid-Latitude Ionosphere 2. Theoretical Framework, *J. Geophys. Res.,* 96, 3747-3753, 1991.
24. Kelley, M.C., Haldoupis, C., Nicolls, M. J., Makela, J.J., Belehaki, A., Shalimov, S., and Wong, V. K., Case studies of coupling between the E and F regions during unstable sporadic-E conditions, *J. Geophys., Res*., 108, A12, 1447, doi:10.1029/2003JA009955, 2003.

25. Kazimirovsky, E.S., Coupling from below as a source of ionospheric variability: a review, *Annals Geophys*., 45, 1, 2002.

26. Kazimirovsky, E.S., Herraiz, M., De La Morena, B.A., Effects on the ionosphere due to phenomenon occurring below it: a review, *Surveys in Geophys*., 24, 139-184, 2003.

27. Klenzing, J., Simoes, F., Ivanov, S., Heelis, R.A., Bilitza, D., Pfaff, R., and Rowland, D., Topside equatorial ionospheric density and composition during and after extreme solar minimum, *J. Geophys. Res*., 116, A12330, doi:10.1029/2011JA017213, 2011.

28. Kotake, N., Otuska, Y., Ogawa, T., Tsugawa, T., and Saito A., Statistical study of medium-scale traveling ionospheric disturbances observed with the GPS networks in Southern California, *Earth Planets Space*, 59, 95-102, 2007.

29. Lastovicka, J., Forcing of the ionosphere by waves from below, *J.Atmos. Solar-Terres. Physics*, 68, 479-497, 2006.

30. Lay, E. H., Shao, X-M., and Carrano, C.S., Varation in total electron content above large thunderstorms, *Geophys. Res. Letters*, 40, 1945-1949, doi:10.1002/grl.50499, 2013.

31. Lay, E. H., Shao, X-M., Kendrick, A.K., and Carrano, C.S., Ionospheric acoustic and gravity waves associated with midlatitude thunderstorms, *J. Geophys. Res*., 10.1002/2015JA021334, 2015.

32. Martinis, C., Baumgardner, J., Wroten J., and Mendillo, M., Seasonal dependence of MSTIDs obtained from 630.0 nm airglow imaging at Arecibo, *Geophys. Res. Lett*., 37, L11103, doi:10.1029/2010GL043569, 2010.

33. Mathews, J.D., and Harper, R.M., Incoherent scatter radar observations of spread-F producing ionospheric structures at Arecibo, *J. Atmos. Terr. Phys*., 34, 1119-1127, 1972.

34. Nygrén, T., Aikio, A.T., Voiculescu, M., and Cai, L., Radar observations of simultaneous traveling ionospheric disturbances and atmospheric gravity waves. *J. Geophys. Res.*, 120, 3949–3960. doi:10.1002/2014JA020794, 2015.

35. Oliver, W.L., et al., Middle and upper atmosphere radar observations of ionospheric density gradients produced by gravity wave packets, *J. Geophys. Res*., Vol 99, No. A4, 6321-6329, 1994.

36. Perkins, F., Spread F and Ionospheric Currents, *J. Geophys. Res*., 78, 218-226, 1973.

37. Pulinets, S.A., and Liu, J.Y., Ionospheric variability unrelated to solar and geomagnetic activity, *Adv. Space Res*., 34, 1926-1933, 2004.

38. Rishbeth, H., F-region links with the lower atmosphere? *J. Atmos. Solar-Terres. Phys*., 68, 469-478, 2006.

39. Rishbeth, H., and Davis, C.J., The 70th anniversary of ionospheric sounding, *Engineering science and education journal*, 139-144, 2001.

40. Tsunoda, R. T., Control of the seasonal and longitudinal occurrence of equatorial scintillations by the longitudinal gradient in integrated E region Pederson conductivity, *J. Geophys. Res.,* 90, A1, 447-456, 1985.

41. Tsunoda, R. T., On the coupling of layer instabilities in the nighttime midlatitude ionosphere, *J. Geophys. Res.,*111, A11304, doi:10.1029/2006JA011630, 2006.

42. Vadas, S.L., Horizontal and vertical propagation and dissipation of gravity waves in the thermosphere from lower atmospheric and thermospheric sources, *J. Geophys. Res*., 112, A06305, doi: 10.1029/2006JA011845, 2007.

43. Vadas, S.L., and Liu, H.-L., The generation of large-scale gravity waves and neutral winds in the thermosphere from the dissipation of convectively generated gravity waves, *J. Geophys. Res*., 114, A10310, doi: 10.1029/2009JA014108, 2009.

44. Yokoyama, T., Hysell, D.L., Otsuka, Y., and Yamamoto, M., Three-dimensional simulation of the coupled Perkins and Es-layer instabilities in the nighttime midlatitude ionosphere, *J. Geophys. Res*., 114, A03308, doi:10.1029/2008JA013789, 2009.

45. Walterscheid, R. L.,Schubert, G., and Brinkman, D. G., Small-scale gravity waves in the upper mesosphere and lower thermosphere generated by deep tropical convection, *J. Geophys., Res.,* 106, D23, 31825-31832, 2001.

46. Wickwar, V.B., and Carlson, H.C., Ionospheric and thermospheric couplings: vertical, latitudinal and longitudinal, *J. Atmos. Solar-Terres*., 61, 141-152, 1999.

47. Figure1 coastline information obtained from: http://www.ngdc.noaa.gov/mgg_coastline/.